Article ID: 1006-8775(2016) 02-0046-11

INFLUENCES OF LOW-FREQUENCY MOISTURE TRANSPORTATION ON LOW FREQUENCY PRECIPITATION ANOMALIES IN THE ANNUALLY FIRST RAINY SEASON OF SOUTH CHINA IN 2010

LI Li-ping (李丽平)[1], XU Guan-yu (许冠宇)[1, 2], NI Bi (倪　碧)[1], LIU Yan-ju (柳艳菊)[3]

(1. Ministry of Education Key Laboratory of Meteorological Disaster of Cooperation of Ministries and Provincial Governments/College of Atmospheric Sciences, NUIST, Nanjing 210044 China; 2. Wuhan Central Meteorological Observatory, Wuhan 430074 China; 3. National Climate Center, Beijing 100081 China)

Abstract: 85-station daily precipitation data from 1961—2010 provided by the National Meteorological Information Center and the NCEP/NCAR 2010 daily reanalysis data are used to investigate the low-frequency variability on the precipitation of the first rain season and its relationships with moisture transport in South China, and channels of low-frequency water vapor transport and sources of low-frequency precipitation are revealed. The annually first raining season precipitation in 2010 is mainly controlled by 10–20 d and 30–60 d oscillation. The rainfall is more (interrupted) when the two low-frequency components are in the same peak (valley) phase, and the rainfall is less when they are superposed in the inverse phase. The 10–20 d low-frequency component of the moisture transport is more active than the 30–60 d. The 10–20 d water vapor sources lie in the South India Ocean near 30° S, the area between Sumatra and Kalimantan Island (the southwest source), and the equatorial middle Pacific region (the southeast source), and there are corresponding southwest and southeast moisture transport channels. By using the characteristics of 10–20 d water vapor transport anomalous circulation, the corresponding low-frequency precipitation can be predicted 6 d ahead.

Key words: low-frequency precipitation characteristics; wavelet analysis; low-frequency vapor sources; annually annually first rainy season of South China

CLC number: P426.6 **Document code:** A

doi: 10.16555/j.1006-8775.2016.S1.005

1 INTRODUCTION

Low-frequency variation of the atmosphere includes intraseasonal oscillation (ISO) (30–60 d) and quasi-biweekly oscillation (QBW) (10–20 d) (Li[1]). Large-scale atmospheric circulation anomalies are the direct cause of precipitation anomalies (Dao and Hsu[2]). Low frequency oscillation is closely related to precipitation anomalies, which are an important aspect of large-scale atmospheric circulation anomalies. Jones[3] and Bond and Vecchi[4] showed that the phase variation of ISO was closely related to precipitation intensity in North America. Barlow et al.[5] indicated that the ISO activities in the Eastern Indian Ocean could regulate the winter precipitation in southwest Asia and had significant inter-annual variation characteristics. The analysis performed by Pohl et al.[6] showed that there was significant ISO in outgoing long-wave radiation (OLR) in South Africa. When large-scale convective cloud clusters propagated eastwardly and northwardly toward that region, there was significant dry-wet phase alternation in the corresponding precipitation field. A study conducted by Wheeler et al.[7] also showed that in southern Australia, tropical convective anomalies were the most direct factor that affected precipitation, except in winter. In addition, different propagation phases with ISO indices had different effects on precipitation in Australia. Zhang et al.[8] noted that the rain belt in southeast China had a significant variation on the intraseasonal time scale, from strengthening to weakening, which was related to the migration of the

Received 2014-09-02; **Revised** 2016-03-03; **Accepted** 2016-07-15

Foundation item: 973 Program (2015CB453202); Specific Project on Public Fields (GYHY201406024); Key National Natural Science Foundation of China (41330425); Third-level Talent Training Project of the Fourth "333 project" in Jiangsu Province; Priority Academic Program Development of Jiangsu Higher Education Institutions (PAPD)

Biography: LI Li-ping, Ph.D., Associate Researcher, primarily undertaking research on regional air-sea interaction and intraseasonal oscillation.

Corresponding author: LI Li-ping, e-mail: li.liping@163.com

convective center of ISO from the Indian Ocean to the West Pacific. The aforementioned studies indicated that globally, low-frequency oscillations of the atmosphere in different regions were closely related to precipitation. Many researchers have studied precipitation process forecasting over an extended range (Lo and Hendon[9]; Wheeler and Hendon[10]; Jones et al.[11]; Galin[12]; Sun et al.[13]). Sun et al. [13] used low-frequency weather charts to analyze the characteristics of low-frequency weather system activity in key regions, based on which they forecasted the precipitation processes in Shanghai and obtained good results.

South China is also a region where heavy precipitation frequently occurs. The pluvial period includes a annually first rainy season (RS) from April to June and a second rainy season from July to September. Polar front precipitation is prominent during the RS, and tropical weather and climate system precipitation is prominent during the second rainy season (Wu and Liang[14]). Low-frequency oscillations in the atmosphere are an important factor that affects low-frequency precipitation anomalies during the rainy season in South China. A study conducted by He and Wen[15] showed that the 850 hPa, 10–20 d low-frequency wind field had an important effect on 10–20 d low-frequency precipitation. In addition, 6 d before and after the 10–20 d precipitation peak, the movement of the wave train in the 200 hPa, 10–20 d low-frequency wind field was closely related to spring precipitation in southeast China. The study conducted by Luo et al.[16] showed that the flash-flood producing rainstorms during the RS in the Xijiang River Basin were the result of the convergence of low-frequency warm-wet flows from the low-latitude ocean and low-frequency dry-cold flows from high latitudes. A study conducted by Ji et al.[17] showed there was prominent QBW and a relatively weak ISO in the precipitation of the RS in Guangdong and the key area of the 500 hPa height field during most years. In addition, two elements were most closely related to one another on the 10–20 d scale: the time for oscillation advance or delay was within 2 d. A study conducted by Zheng et al.[18] showed that rainy season precipitation in South China had a 30–60 d low-frequency cycle. The strong (weak)-to-weak (strong) evolution processes of the Mascrene High and Australian High systems in the Southern Hemisphere corresponded to the migration of the rainy belt in South China from southwest (northeast) to northeast (southwest). A study conducted by Zhang et al.[19] showed that the migration of the active center of ISO from the Indian Ocean to the West Pacific generated less precipitation in South China. In addition, studies about individual years conducted by other researchers showed that the locations and propagation of low-frequency systems were closely related to the precipitation volume in South China (Xin et al.[20] ; Tong et al.[21]; Sun et al.[22]; Lin et al.[23]).

During the 50-year period from 1961 to 2010, except 1973, the precipitation in the RS in South China in 2010 was abnormally more than average (figure omitted). Precipitation in 2010 showed such characteristics as less precipitation during the early rainy season and more precipitation later in the year. Twelve heavy rainfalls occurred from April to June, and the total rainfall in some regions reached a level that only occurs once every 500 years. These rainfalls significantly affected agriculture and traffic in South China; however, there are few studies on the low-frequency characteristics and genesis of this heavy rainfall process. Because water vapor transport anomalies are an important physical factor that affects winter and spring precipitation anomalies in South China (Wu et al.[24]), we focused on analyzing the low-frequency characteristics of precipitation during the RS in South China in 2010. We further studied the relationship between the low-frequency precipitation and low-frequency water vapor transport, investigated the source region of low-frequency water vapor transport, and provided clues for the extended range precipitation forecast during the RS in South China.

2 DATA AND METHODS

The data used in this study include (1) the 2010 global National Centers for Atmospheric Prediction (NCEP)/National Center for Atmospheric Research (NCAR) daily reanalysis data (including zonal wind (u), meridional wind (v), and specific humidity data) (resolution: 2.5˚×2.5˚) and (2) the daily precipitation data recorded at 753 stations from 1961 to 2010 provided by the National Meteorological Information Center (China). The 106–120˚E, 20–27.5˚N region was selected as the South China region for this study. Stations with less than 50 years of precipitation data were eliminated. A total of 85 stations were selected to represent South China (Fig. 1).

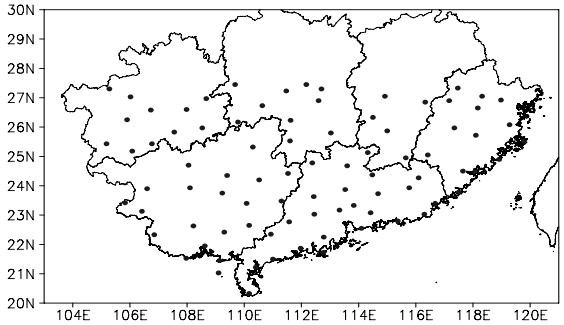

Figure 1. Locations of 85 stations in South China.

The Morlet wavelet analysis method (Wu and Wu[25]) was used to analyze the prominent period of

precipitation and water vapor flux during the RS in South China. In addition, a Butterworth Band-pass Filter (Wu and Wu[25]) was used to filter the prominent period.

3 ANALYSIS OF THE LOW-FREQUENCY PRECIPITATION CHARACTERISTICS OF THE ANNUALLY FIRST RAINY SEASON IN SOUTH CHINA

3.1 *Selection of representative stations*

For the spatial distribution of the total precipitation (Fig. 2a) and its of anomalies (Fig. 2b) during the RS in 2010, precipitation was primarily concentrated in a large region of Fujian, central and southern Jiangxi, a large region of Guangdong, central and eastern Guangxi, and central and southern Hunan. The precipitation at the junction of Jiangxi and Fujian, Guangdong, and northern Guangxi was over 300 mm higher than the precipitation during the identical period in a normal year. Comprehensively considering the large value areas of total precipitation, areas of significantly increased precipitation (areas where the precipitation anomaly was more than 200 mm), and the relative homogeneity of station distribution, 22 representative stations were selected from the 85 stations as the key study objects, and the low-frequency precipitation characteristics at these 22 stations were studied.

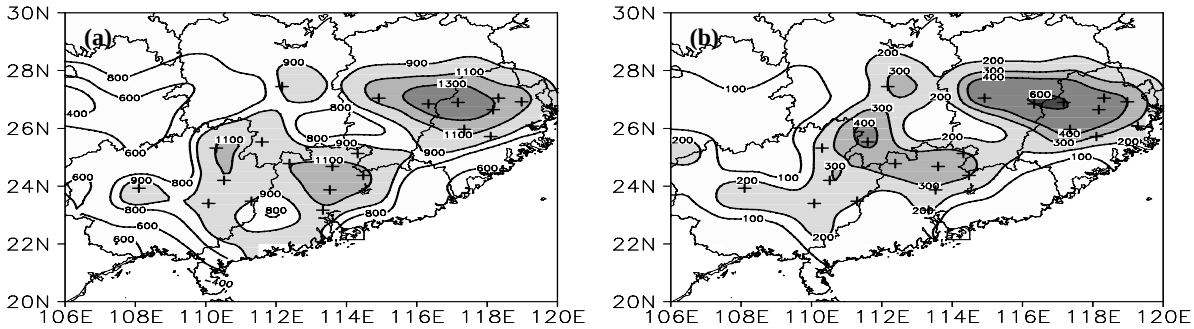

Figure 2. Accumulated rainfall totals (a, shaded area≥900 mm) and rainfall anomaly (b, shaded area≥200 mm) in the annually RS in South China, "+"denotes the 22 representative stations. Units: mm.

3.2 *Low-frequency precipitation characteristics*

To determine whether precipitation during the annually RS in South China had a significantly low-frequency cycle, a Morlet wavelet analysis was performed on the 2010 daily precipitation series from the 22 representative stations. Table 1 lists the statistical results of the prominent periods. Low-frequency periods of more than 10 d were prominent. Overall, 10–20 and 30–60 d were the two prominent precipitation oscillation periods during the RS in South China in 2010.

Table 1. Main oscillation periods of precipitation on the 22 representative stations from April to June of 2010 in South China.

station	period/d	station	period/d	station	period /d
Fuzhou	10–20; 30–60	Jian	10–50	Daoxian	10–15; 30–60
Pingnan	30–50	Nanxiong	10–25; 30–50	Guilin	10–15; 30–70
Jianou	10–20; 30–50	Saoguan	10–20; 30–50	Wuzhou	10–30
Nanping	10–15; 25–60	Lianping	10–30; 30–55	Guiping	10–20; 25–40
Jiuxianshan	10–20; 30–50; 60–80	Fugang	10–20; 30–50	Menshan	10–30
Yongan	10–20; 30–50; 60–70	Lianxian	10–20; 30–50	Douan	10–30; 45–70
Taining	15–70	Guangzhou	10–20	stations Average	10–20; 30–50
Guangchang	10–70	Shuangfeng	10–30; 40–50		

Figure 3 shows the wavelet analysis results of the regional mean daily precipitation series of the 22 representative stations during the RS in South China. The 10–20 d cycle was more prominent from May to June, whereas the 30–60 d cycle was prominent from April to June (Fig. 3a). Based on calculations, the 10–20 d and 30–60 d low-frequency precipitation cycles represented 27.7 and 34% (total variance percentage), respectively, of the 10–90 d total low-frequency precipitation. The 30–60 d low-frequency component corresponded to the precipitation process. The 10–20 d low-frequency component reflected the precipitation intensity variation during each precipitation process (Fig. 3b). Additionally, when the 10–20 d and 30–60 d low-frequency components superposed one another in the positive phase, there was relatively more precipitation, and when the 10–20 d and 30–60 d low-frequency components superposed one another in the negative phase, precipitation ceased. When the 10–20 d and 30–60 d low-frequency components superposed one another out of phase, the precipitation

was relatively weak.

4 LOW-FREQUENCY CHARACTERISTICS OF WATER VAPOR FLUX DURING THE ANNUALLY FIRST RAINY SEASON IN SOUTH CHINA

Water vapor fluxes can reflect circulation characteristics and the water vapor source of precipitation. Therefore, it is important to understand the relationship between low-frequency water vapor fluxes and low-frequency precipitation during the RS.

The distribution of the correlation coefficients between the regional mean precipitation series during the RS in South China and the 850 hPa zonal (*QU*) , meridional (*QV*) water vapor fluxes respectively (Fig. 4) showed that when larger northeasterly (20–30˚N) and northwesterly (35–40˚N) cold water vapor fluxes from northern South China occurred with larger southwest warm water vapor fluxes from the Arabian Sea-Bay of Bengal-South China coast, more precipitation occurred in South China.

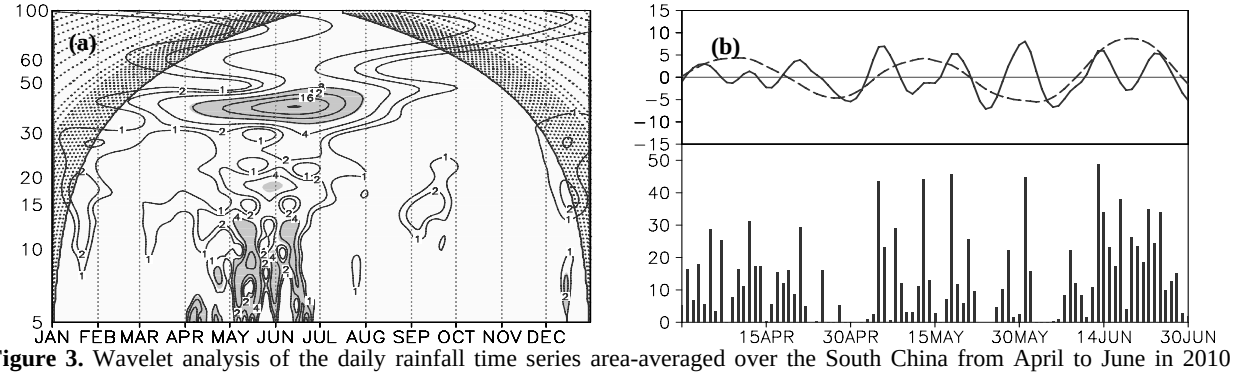

Figure 3. Wavelet analysis of the daily rainfall time series area-averaged over the South China from April to June in 2010 (a, shaded area is significant at the $\alpha = 0.05$ level) and the daily rainfall time series (b, histogram, units: mm) and their 10-20 d (solid line, units: mm) and 30-60 d (dashed line, units: mm) filtered components.

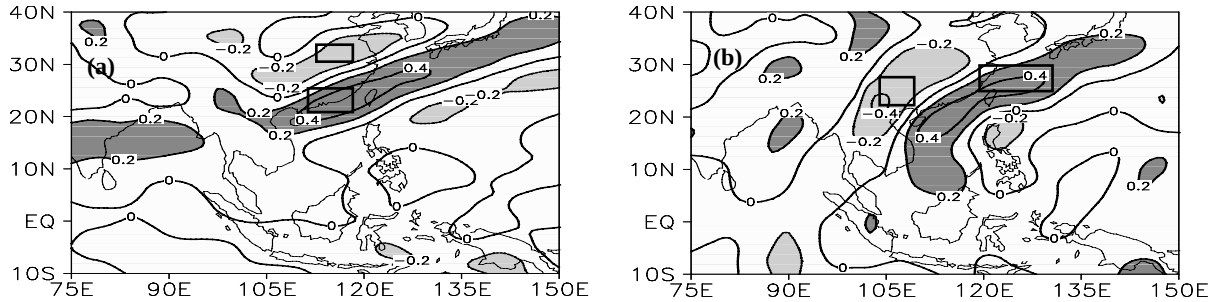

Figure 4. The correlation coefficients between the unfiltered daily rainfall time series averaged over the South China and unfiltered daily 850hPa zonal (a) and meridional (b) vapor flux (shaded area is significant at the $\alpha = 0.05$ level) respectively.

Regional water vapor fluxes (black boxes in Figs. 4a and 4b) that were positively and negatively correlated to precipitation during the RS in South China were selected. The water vapor fluxes in the positively and negatively correlated areas were averaged regionally. The differences were defined as the zonal (*QUI*) and meridional (*QVI*) water vapor flux indices, i.e.:

$$QUI = QU(112.5–122.5^{\circ}E, 20–25^{\circ}N) - QU(115–122.5^{\circ}E, 30–35^{\circ}N)$$

$$QVI = QV(117.5–130^{\circ}E, 22.5–27.5^{\circ}N) - QV(100–107.5^{\circ}E, 20–25^{\circ}N)$$

From the Morlet wavelet analysis performed on the daily time series of *QUI* and *QVI* (Figs. 5a and 5b), there was a significant 10–20 d low-frequency cycle in the *QUI* in May and mid- and late June and in the *QVI* in mid- and late April and mid- and late May and June. The 30–60 d low-frequency cycle of the meridional water vapor flux was significant at $\alpha = 0.1$ (figure omitted), thus indicating that compared to the 30–60 d low-frequency component, the 10–20 d low-frequency component of the water vapor flux contributed more significantly to precipitation in the identical frequency domain. Therefore, the relationship between the 10–20 d low-frequency water vapor flux and low-frequency precipitation was subsequently analyzed. When the 10–20 d band-pass-filtered *QUI* and *QVI* and low-frequency precipitation series (Fig. 5c) were compared and an amplitude greater than 0.5 standard deviations was used as the critical value, 5 full cycles of 10–20 d low-frequency precipitation occurred since April 19. In addition, during these 5 cycles, the peaks and valleys of the low-frequency precipitation corresponded to those of *QUI* and *QVI.*

5 EFFECT OF LOW-FREQUENCY WATER

VAPOR FLUXES ON LOW-FREQUENCY PRECIPITATION

To understand the effect of low-frequency water vapor transport on low-frequency precipitation, each cycle was divided into 8 phases according to previous studies (Chan et al.[26]; Mao and Wu[27]). Phase 1 (5) represents the oscillation transition from the interruption (active) period to the active (interruption) period, phase 3 represents the peak of the active period, and phase 7 represents the valley of the interruption period. After each cycle is completed, it returns to phase 1. In Fig. 5c, phases 1, 3, 5, and 7 are marked in the first cycle. Phases 2, 4, 6, and 8 represent half of the time required for the oscillation amplitude to reach the maximum or minimum value of the cycle. The phase definitions in the other cycles were identical. Thus, the effect of the low-frequency water vapor transport variation on low-frequency precipitation was analyzed through the evolution of 8 phases.

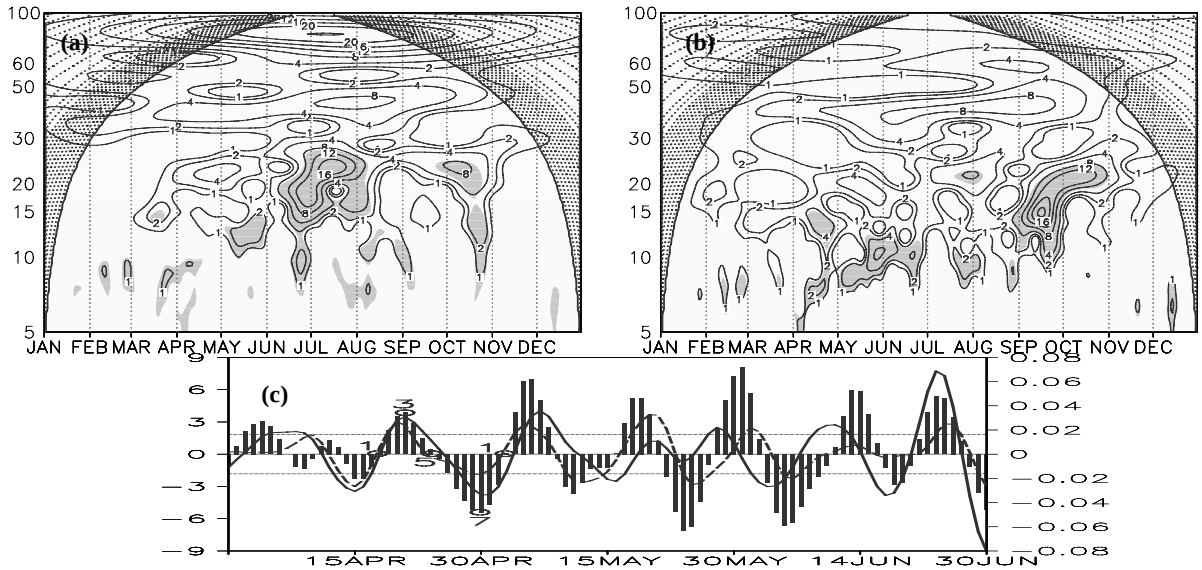

Figure 5. Wavelet analysis of 850hPa zonal (a) and meridional (b) vapor flux index daily time series from January to December in 2010 (shaded areas are significant at the $\alpha = 0.05$ level) and the daily 10-20 d filtered rainfall time series from April to June in 2010 (histogram, units: mm, left coordinate) and the filted *QUI* (solid line), *QVI* (dashed line) series (units: $kg\cdot(m\cdot s)^{-1}$, right coordinate), dotted line is 0.5 times standard deviation of filtered precipitation time series, 1, 3, 5 and 7 denotes low frequency oscillation phase respectively (c).

5.1 *Synthesized phase fields of the 850 hPa 10–20 d low-frequency water vapor flux*

Figure 6 shows the low-frequency water vapor flux fields of the 8 phases synthesized from 10–20 d low-frequency precipitation. Prior to heavy rainfalls (Fig. 6a, phase 1), the low-frequency anticyclonic water vapor circulation was strong in the Mascarene region, which significantly strengthened the cross-equatorial water vapor flow from Somalia. The cross-equatorial water vapor flow from Somalia converged with the westerly water vapor flow from the south of the cyclonic water vapor circulation of the Arabian Sea and Bay of Bengal at the southern end of the Indian peninsula. The flow was then transported east and converged with the easterly water vapor flow from the south of the South China Sea-West Pacific anticyclonic water vapor circulation to the west of the Indo-China Peninsula. The flow was then transported northeast along the southeastern coast of China. There was weak cyclonic water vapor circulation east of Baikal Lake and strong anticyclonic water vapor circulation on the ocean east of the Japan Sea. The east- and westward cold water vapor flows of these two cyclonic and anticyclonic water vapor circulations converged with the warm water vapor flow in the Jianghuai region, which caused more precipitation in this region. Subsequently (Fig. 6b, phase 2), the northward movement of the anticyclonic water vapor circulation from the Mascarene region was continuously intensified. The cross-equatorial water vapor flow from Somalia passed the Indochina Peninsula and converged with the warm-wet flow on the northwestern side of the southward moving South China Sea-West Pacific anticyclonic water vapor circulation, whose westward extension was intensified. The warm-wet flow converged with the intensified and southward-moving northward flow on the western side of the cyclonic circulation from eastern Baikal Lake and the eastward cold flow on the southern side of the anticyclonic circulation from east of the Japan Sea at the Yangtze River Basin, which increased the low-frequency precipitation in the region. In the extremely active

phase (Fig. 6c, phase 3), the cross-equatorial water vapor flow from Somalia continued to transport water vapor to South China via the Arabian Sea and Bay of Bengal. The anticyclonic water vapor circulation of the South China Sea-West Pacific and the anticyclonic water vapor circulation east of the Japan Sea were connected, and the southward warm water flow on its northwestern side converged with the southwest warm water vapor from Somalia. Together, the connected flow converged with the northward cold flow on the western side of the southward-moving cyclonic circulation from eastern Baikal Lake that propagated over South China, which enabled low-frequency precipitation to easily form in South China. In phase 4 (Fig. 6d), the low-frequency anti-cyclonic water vapor circulation from the Mascarene region significantly weakened. The cross-equatorial water vapor flow from Somalia was terminated at the Indochina Peninsula. The South China Sea-West Pacific anticyclonic water circulation weakened and moved out of South China, and the cyclonic water vapor circulation from eastern Baikal Lake continued to move east- and southward. The entire South China region was controlled by a northward flow, and low-frequency precipitation weakened in South China. When transitioning from the active to the interruption period (phase 5, Fig. 6e), the form of the water vapor circulation was nearly opposite to that in phase 1, and the subsequent evolution was also similar to phase 2 through phase 4, but the direction of water vapor transport was opposite. In particular, during the interruption period (phase 7, Fig. 6g), South China was at the center of an anticyclonic water vapor transport circulation and was the water vapor transport divergence area. Thus, low-frequency precipitation was interrupted. The intraseasonal and seasonal variations of the Mascarene High significantly affected East Asian summer monsoon precipitation (Xue et al.[28]; Xue et al. [29]). The low-level jet over Somalia was most important for the water vapor transport between the two hemispheres and significance for East Asian summer climate predictions (Wang and Xue[30]).

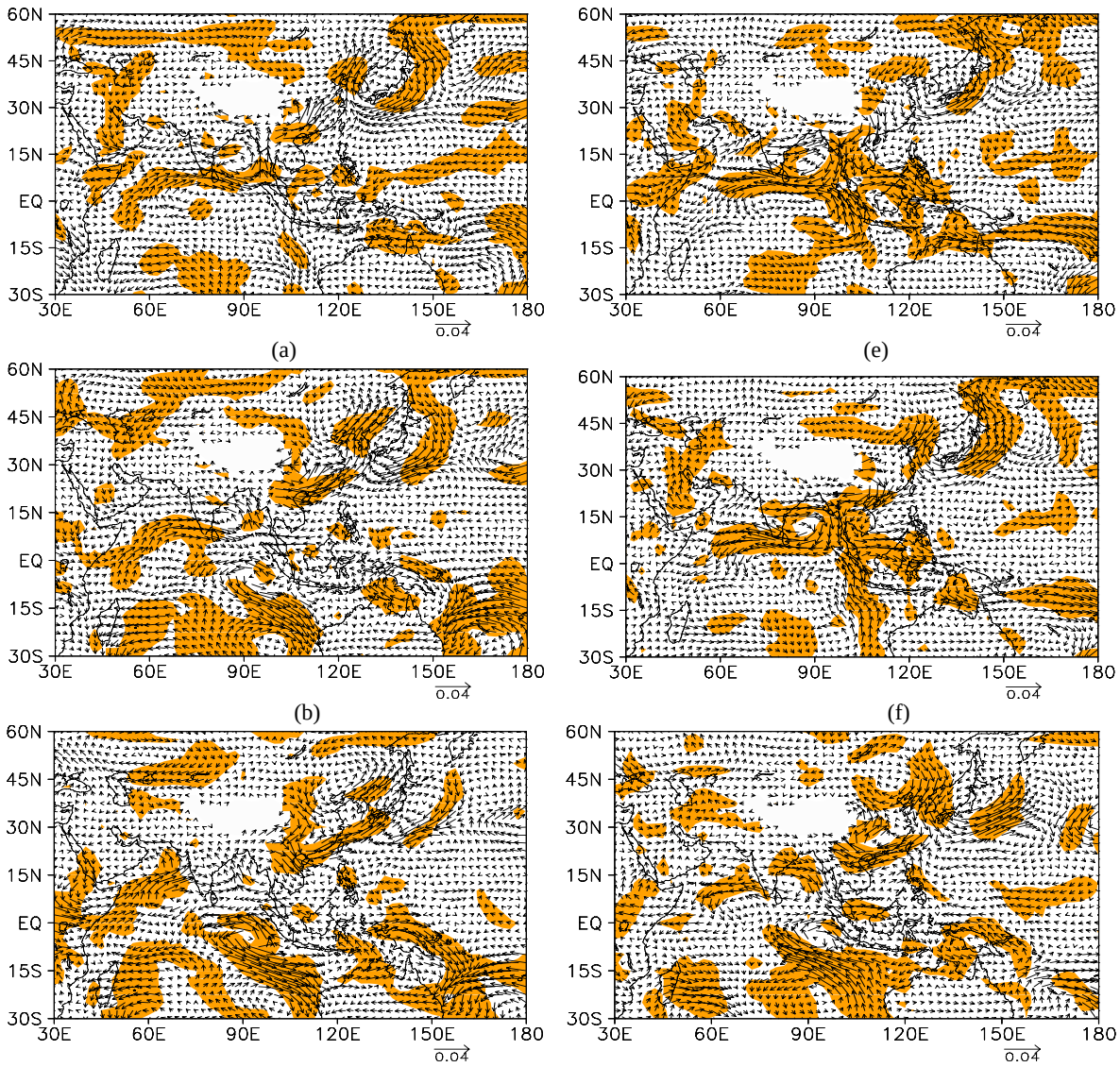

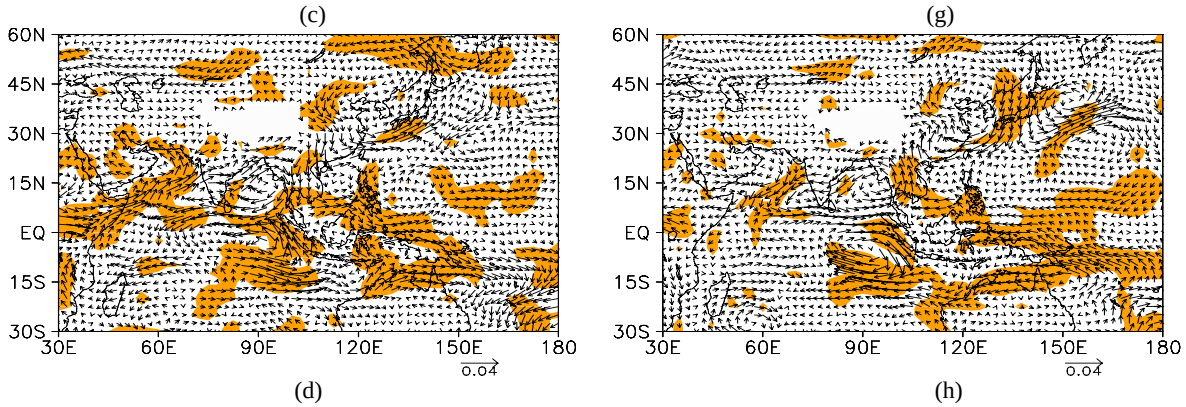

Figure 6. Synthesis of the 10–20 d low-frequency water vapor flux fields of phases 1–8 at 850 hPa (see Fig. 5c) (a–h). Unit: kg/(m·s). The shaded areas indicate an $a = 0.05$ significance.

The aforementioned studies further confirmed the key roles of the Mascarene High and low-level jet over Somalia in the formation of 10–20 d low-frequency precipitation. Next, we further discuss the prediction significance of the water vapor transport accompanied by these two circulation systems in the formation of low-frequency precipitation during the RS in South China.

5.2 *Source region of the 10–20 d low-frequency water vapor transport*

Through an analysis of the delay-dependent relationship between low-frequency water vapor transport flux and low-frequency precipitation, we can understand the propagation characteristics of the low-frequency water vapor flux that affects low-frequency precipitation and show the low-frequency water vapor source region that caused low-frequency precipitation.

For the 10–20 d low-frequency oscillation, the time interval of the low-frequency water vapor transport field was 8 d (-8 d) ahead of the low-frequency precipitation field, and an 8-d (+d) delay was approximately one full 10–20 d low-frequency oscillation cycle (quasi-15 d). In terms of the spatial distribution characteristics of the time-delay correlation coefficients (Fig. 7), the distribution of the left column (advance) was basically the opposite of the distribution of the right column (delay) in Fig. 7.

The simultaneous correlation distribution of the low-frequency zonal water vapor flux and low-frequency precipitation (shadows in Fig. 7) shows that the Somalia-south of the Arabian Sea-north of the Indochina Peninsula-South China coast and the South China Sea-West Pacific-southwest Baikal Lake regions were positively correlated. The South Indian Ocean east of Madagascar and the subtropical region in East China were negatively correlated regions. The correlation coefficients of the low-frequency meridional water vapor flux and low-frequency precipitation (contours in Fig. 7), and background water transport circulation field (0 d) showed that the stronger the low-frequency anticyclonic water vapor transport circulation in the Mascarene region was, the stronger the cross-equatorial water vapor flow that passed Somalia from the South Indian Ocean was, and the more the low-frequency warm water vapor was transported via the Arabian Sea-Bay of Bengal-South China region. The stronger the anticyclonic water vapor transport circulation over the South China Sea-West Pacific was, the more southwest warm water vapor that was transported to South China, and the more beneficial it was to increased precipitation in South China. Convergence of the south and north warm-cold water vapor transport circulations in South China was benefitted by a stronger northwest cold flow from the west, southeast of Baikal Lake, and a northeast cold flow from the subtropical region in East China, which caused more low-frequency precipitation in South China.

From the propagation of a significant correlation region of zonal water vapor flux (Fig. 7), Madagascar, the ocean southeast of Madagascar and north of the Bay of Bengal, and the region between Sumatra and Kalimantan were significant, positively correlated regions of zonal water vapor flux at -8 d. From -6 to -4 d, the positive correlation region from southern Africa to Madagascar moved northeastwardly to the southern Arabian Sea, and the positive correlation region west of Sumatra moved to the southern Bay of Bengal. Thus, a Madagascar-Arabian Sea-Bay of Bengal positive correlation belt was formed, which strengthened eastward water vapor transport. In addition, the significant negative correlation belt south of the Philippine archipelago was enlarged, which indicated that the South China Sea-West Pacific anticyclonic water vapor transport circulation was strengthened. At -2 d, the positive correlation region north of Madagascar moved northeastwardly to the east of Somalia, connected with the positive correlation region of the Arabian Sea, and then continued to move northeastwardly to South China

and the coastal region. The significant, negatively correlated region near the Philippine archipelago propagated northwardly to the South China Sea, thus indicating that the South China Sea-West Pacific anticyclonic water vapor transport circulation transported more water vapor to South China. At 0 d, the positively correlated region in South China was even larger, which indicated that the low-frequency water vapor transported from Somaliavia the Arabian Sea and Bay of Bengal and from the South China Sea-West Pacific to South China were stronger.

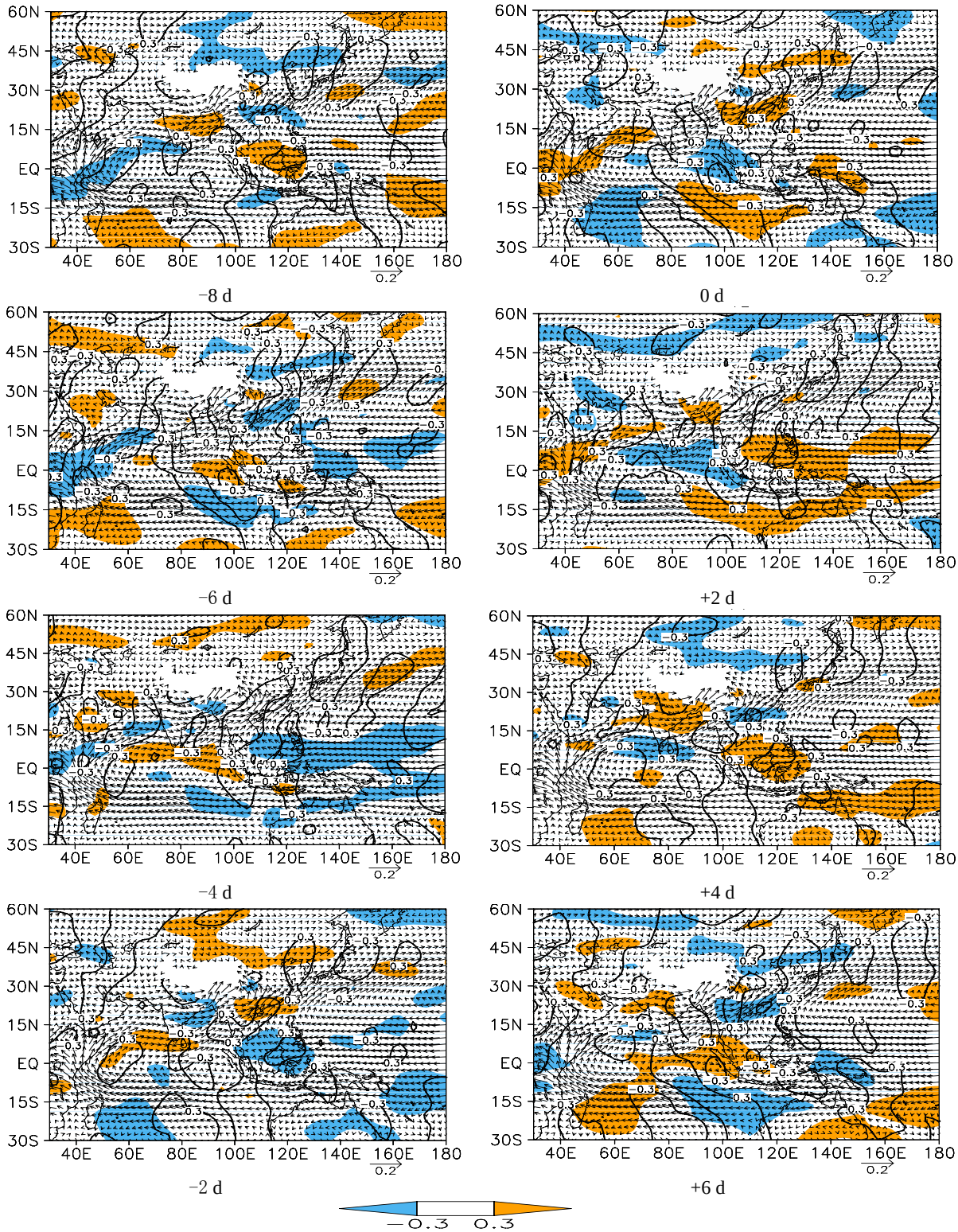

Figure 7. The time-delay correlation coefficients of the 10–20-d filtered time-series of low-frequency precipitation in the RS in South China and the 10–20-d filtered 850 hPa low-frequency water vapor transport flux. The shadows and contour zones correspond to regions where the correlation coefficients of low-frequency precipitation and low-frequency zonal fluxes and of low-frequency

precipitation and meridional fluxes were significant at $a = 0.05$ level. The negative (positive) time-delay days at the top left corner of each figure represent that the water vapor transport flux is ahead of (behind) the low-frequency precipitation. The vector field is the mean water vapor flux from April to June.

During the aforementioned processes, there was an association between the gradual transport of a cold-water flow from mid-high latitudes and the subtropical region in East China to South China. The distribution of significantly correlated regions of low-frequency precipitation and low-frequency meridional water vapor flux (Fig. 7) indicated that warm water flowed from southwest (the Indian Ocean direction) and southeast (the South China Sea-West Pacific direction) converged with the northwest cold water flow from mid-high latitudes (mainly cold air) and the northeast cold water flow from the subtropical region in South China, which caused more low-frequency precipitation in South China. From +2 to +6 d, negatively correlated regions propagated in South China along low, southwestern latitudes and mid-high, northern latitudes, which generated low-frequency water vapor transport channels. A positive correlation belt propagated in the South China Sea via the equatorial Central Pacific. South China was in a water vapor divergence zone, and low-frequency precipitation gradually decreased, thus completing a full cycle.

6 CONCLUSIONS

In this study, we studied the simultaneous and time-delay correlations between the 10–20 d low-frequency water vapor flux and low-frequency precipitation in the RS in South China and showed the low-frequency water vapor source regions and transport channels that affected the low-frequency precipitation in the RS in South China.

(1) There were significant 10–20 d and 30–60 d low-frequency cycles for precipitation in the RS in South China. The 30–60-d low-frequency component corresponded to the precipitation process, whereas the 10–20 d low-frequency component reflected the variation in precipitation intensity during the precipitation process. The superposition of the peak phases of the two low-frequency components corresponded to the precipitation peak, and the superposition of the valley phases corresponded to the precipitation interruption. The superposition of opposite phases corresponded to weak precipitation. The 10–20 d low-frequency components of zonal and meridional water vapor fluxes in the RS in South China were significantly stronger than the 30–60-d low-frequency components.

(2) The low-frequency water vapor transport circulation systems that affected the 10–20 d low-frequency precipitation included the anticyclonic (cyclonic) water vapor circulation from the Mascarene region, the cross-equatorial water vapor flow from Somalia (together known as the southwest water vapor circulation system), and the anticyclonic (cyclonic) water vapor circulation from the South China Sea-West Pacific (together known as the southeast water vapor circulation system). These water vapor circulation systems generated water vapor environments that were beneficial (detrimental) to low-frequency precipitation in South China through variations in location and intensity.

(3) There were two major source regions of low-frequency water vapor transport that affected the 10–20 d low-frequency precipitation in South China: the southwest source region in the South Indian Ocean (near 30˚S) and between Sumatra and Kalimantan near the equator and the southeast source region in the equatorial Central Pacific, from which two low-frequency water vapor transport channels were formed, i.e., the southwest low-frequency warm water vapor transport channel (South Indian Ocean-Somalia-Arabian Sea-Bay of Bengal-South China) and the southeast water vapor channel (equatorial Central Pacific-Philippine archipelago-South China Sea-South China) formed from the east-west extension and southwest displacement of the anticyclonic circulation from the South China Sea-West Pacific. Abnormal low-frequency water vapor transport occurred in the southwest source region 8 d before low-frequency precipitation. The abnormal characteristics were more prominent in these two water vapor source regions 6 d before low-frequency precipitation. Therefore, it is possible to predict low-frequency precipitation 6 d before the occurrence of low-frequency precipitation by observing and analyzing the low-frequency characteristics of water vapor transport circulations in these two source regions.

REFERENCES:

[1] LI Chong-yin. Atmosphere low-frequency oscillation [M]. Beijing: China Meteorological Press, 1991 (in Chinese).

[2] DAO Shih-yen, HSU Shu-ying. Some aspects of the circulation during the periods of the persistent drought and flood in Yangtze and Hwai-ho valleys in summer [J]. Acta Meteorolog Sinica, 1962, 32(1): 1-10.

[3] JONES C. Occurrence of extreme precipitation events in California and relationships with the Madden-Julian oscillation [J]. J Climate, 2000, 13(20): 3 576-3 587.

[4] BOND N A, VECCHI G A. The influence of the Madden-Julian oscillation on precipitation in Oregon and Washington [J]. Wea Forecast, 2003, 18(4): 600-613.

[5] BARLOW M, WHEELER M, LYON B, et al. Modulation of daily precipitation over southwest Asia by the Madden-Julian oscillation [J]. Mon Wea Rev, 2005, 133(12): 3 579-3 594.

[6] POHL B, RICHARD Y, FAUCHEREAU N. Influence of the Madden-Julian oscillation on southern African summer rainfall [J]. J Climate, 2007, 20(16): 4 227-4 242.
[7] WHEELER M C, HENDON H H, CLELAND S, et al. Impacts of the Madden-Julian oscillation on Australian Rainfall and Circulation [J]. J Climate, 2009, 22(6): 1 482-1 498.
[8] ZHANG L N, WANG B Z, ZENG Q C. Impact of the Madden-Julian oscillation on Summer Rainfall in Southeast China [J]. J Climate, 2009, 22(2): 201-216.
[9] LO F, HENDON H H. Empirical extended-range prediction of the Madden-Julian oscillation [J]. Mon Wea Rev, 2000, 128(7): 2 528-2 543.
[10] WHEELER M C, HENDON H H. An all-season real-time multivariate MJO index: Development of an index for monitoring and prediction [J]. Mon Wea Rev, 2004, 132(8): 1 917-1 932.
[11] JONES C, CARVALHO M V, HIGGINS R W, et al. A statistical forecast model of tropical intraseasonal convective anomalies[J]. J Climate, 2004, 17(11): 2 078-2 094.
[12] GALIN M B. Study of the low-frequency variability of the atmospheric general circulation with the use of time-dependent empirical orthogonal functions[J]. Atmos Ocean Phys, 2007, 43(1): 15-23.
[13] SUN Guo-wu, KONG Chun-yan, XIN Fei, et al. Method of extended range forecast of atmospheric low-frequency wave in key region [J]. Plateau Meteorol, 2011, 30(3): 594-599.
[14] WU Shang-sen, LIANG Jian-yin. Temporal and spatial characteristics of the drought and flood during the rainy season in South China [J]. J Trop Meteorol, 1992, 8(l): 87-92 (in Chinese).
[15] HE Jia-jia, WEN Zhi-ping. The influences of the quasi biweekly oscillation on the precipitation in spring in South China [C]. Conference Proceeding on Monsoon Dynamics Forum of the Twenty-sixth China Meteorological Society Annual Meeting. 2009: 56-66.
[16] LUO Qiu-hong, JI Zong-ping, WU Nai-geng, et al. Analyses of intraseasonal oscillation characteristics of flood-causing rainstorms in Xijiang River valley during annually first raining season in the past years [J]. J Trop Meteorol, 2011, 17(2): 136-146.
[17] JI Zhong-ping, GU De-jun, WU Nai-geng, et al. Variations of torrential rain in first rainy season in Guangdong province and Its relationships with the biweekly oscillation of 500 hPa Key region [J]. .J Appl Meteorol Sci, 2010, 21(6): 671-684 (in Chinese).
[18] ZHANG Ting, WEI Feng-ying, HAN Xue. Low frequency oscillations of Southern Hemispheric critical systems and Precipitation during flood season in South China [J]. J Appl Meteorol Sci, 2011, 22(3): 265-274 (in Chinese).
[19] ZHANG Li-na, LIN Peng-fei, XIONG Zhe, et al. Impact of the Madden-Julian oscillation on pre-flood season precipitation in South China [J]. Chin J Atmos Sci, 2011, 35 (3): 560-570 (in Chinese).
[20] XIN Fei, XIAO Zi-niu, LI Ze-chun. Relation between flood season precipitation anomalies in South China and East Asian atmospheric low frequency oscillation in 1997 [J]. Meteorol Mon, 2007, 33(12): 23-30 (in Chinese).
[21] TONG Tin-ngai, WU Chi-sheng, WANG An-yu, et al. An observational study of interaseasonal variations over Guangdong province China during the rainy season of 1999 [J]. J Trop Meteorol, 2007, 23(6): 683-689 (in Chinese).
[22] SUN Dan, JU Jian-hua, LÜ Jun-mei. The influence of the interaseasonal oscillation of the East Asian monsoon on the precipitation in East China in 2003 [J]. J Trop Meteorol, 2008, 24(6): 641-648 (in Chinese).
[23] LIN Ai-lan, ZHENG Bin, GU De-jun, LI Chun-hui, et al. Activity characteristics of East Asian summer monsoon and rainfall distribution over eastern China in 2006 [J]. J Trop Meteorol, 2009, 25(2): 129-140 (in Chinese).
[24] WU Wei, WEN Zhi-ping, CHEN Yun-guang, et al. Interannual variability of winter and spring precipitation in South China and its relation to moisture transport [J]. J Trop Meteorol, 2013, 19(4): 322-330.
[25] WU Hong-bao, WU Lei. Diagnosis and prediction method of Climate variability [M]. Beijing: China Meteorological Press, 2005: 208-225.
[26] CHAN J C L, AI W, XU J. Mechanisms responsible for the maintenance of the 1998 South China Sea summer monsoon [J]. J Meteorol Soc Japan, 2002, 80(5): 1 103-1 113.
[27] MAO Jiang-yu, WU Guo-xiong. Intraseasonal variability in the Yangtze-huaihe river rainfall and subtropical high during the 1991 Meiyu period [J]. Acta Meteorol Sinica, 2005, 63(5): 762-770 (in Chinese).
[28] XUE Feng, LIN Yi-hua, ZENG Qing-cun. On the seasonal division of atmospheric general circulation and its abrupt change. Part III: Climatology [J]. Chin J Atmos Sci, 2002, 26(3): 308-314 (in Chinese).
[29] XUE Feng, WANG Hui-jun, HE Jin-hai. The interannual variability of Mascarene high and Australia high and its influence on East Asian summer monsoon precipitation [J]. Chin Sci Bull, 2003, 48(3): 287-291 (in Chinese).
[30] WANG Hui-jun, XUE Feng. Interannual variability of Somali Jet and its influences on the inter-hemispheric water vapor transport and on the East Asian summer rainfall [J]. Chin J Geophys, 2003, 46(1): 18-25.

Citation: LI Li-ping, XU Guan-yu, NI Bi et al. Influences of low-frequency moisture transportation on low frequency precipitation anomalies in the annually first rainy season of South China in 2010 [J]. J Trop Meteorol, 2016, 22(2): 46-56.